Journal of Solid State Chemistry 182 (2009) 253–258

Contents lists available at ScienceDirect

Journal of Solid State Chemistry

journal homepage: www.elsevier.com/locate/jssc

Magnetic properties of $KNaMSi_4O_{10}$ compounds ($M = Mn, Fe, Cu$)

P. Brandão [a], J. Rocha [a], M.S. Reis [b,*], A.M. dos Santos [c], R. Jin [c]

[a] CICECO and Chemistry Department, Universidade de Aveiro, 3810-193 Aveiro, Portugal
[b] CICECO, Universidade de Aveiro, 3810-193 Aveiro, Portugal
[c] NSSD-MSTD, Oak Ridge National Laboratory, Oak Ridge, TN 37831-6475, USA

ARTICLE INFO

Article history:
Received 7 July 2008
Received in revised form
23 September 2008
Accepted 2 October 2008
Available online 7 November 2008

PACS:
91.25.F–
75.50.Xx
36.40.Cg

Keywords:
Manaksite
Fenaksite
Litidionite
Magnetic properties
Dimers
Hydrothermal synthesis

ABSTRACT

In the present work the synthesis and magnetic properties of three compounds with formula $KNaMSi_4O_{10}$ ($M = Mn, Fe, Cu$) are described. These compounds are synthetic analogs to natural occurring minerals: fenaksite—Fe^{2+}, litidionite—Cu^{2+} and manaksite—Mn^{2+}. The crystal structure consists of complex silicate chains interconnected by edge-sharing MO_5 square pyramids dimerized in M_2O_8 units. This charged metal–silicate framework is compensated by monovalent alkali metals (K^+, Na^+). Despite the isostructural nature of these compounds, and the consequent similarity of the M–O topology, that rules the magnetic properties, these are quite different. While there are antiferromagnetic (AF) interactions within the Mn and Cu dimers (exchange interaction $J = -3.83(1)$ and $-2.86(3)$ K, respectively) with no long range order, a ferromagnetic interaction within Fe dimers ($J = +7.6(1)$ K) is observed with a three-dimensional transition at 9 K to an AF ground state. The magnetic behavior is analyzed using the HDVV (Heisenberg–Dirac–Van Vleck) formalism and discussed in the light of the crystal structure.

1. Introduction

In recent years there have been great strides in the research of molecular magnets. Novel synthetic techniques in both metal–organic and soft inorganic chemistry are providing a wealth of new compounds to investigate. In such compounds, the typically weak magnetic interactions present a wonderful opportunity to study the interplay between the spin, charge and orbital degrees of freedom and how these couple with the lattice [1,2]. Nevertheless, molecular magnets are not only interesting from the fundamental physics point of view, but there is also a reasonable expectation that, stemming from this research, new types of high density magnetic data storage, magnetic sensors at the molecular level [3], and quantum computation chips using the high temperature quantum entanglement effect [4] (and references therein can be developed).

Although molecular magnets are typically organometallic compounds (in which the organic ligands allow the preservation of the magnetic low-dimensional character even at low temperature [5]), there are also purely inorganic systems where notable low-dimensional magnetism phenomena are observed. Examples of this are, for instance, $CuGeO_3$ exhibiting a spin-peierls transition [6] or the Haldane chain compound Y_2NiBaO_5 [7].

One of the fundamental aspects of magnetism is the relationship between the magnetic exchange and the atomic structure. While some general rules governing the superexchange interaction are qualitatively understood from both chemical (occupied orbitals) and geometrical information (bond angles and lengths), through the Goodenough–Kanamori rules [8–10], these interactions are also extremely dependent on a multiplicity of other factors such as the covalency of the bond (or the bridging anionic species), local distortion and, in many instances, next-near neighbor interactions. For this reason, there have been extensive efforts to understand, in a systematic way, to what extent the different structural and chemical parameters affect the sign and magnitude of the magnetic interaction [11,12].

In the present work, the magnetic properties of a series of isostructural transition metal silicates obtained hydrothermally are studied. This synthesis method is applicable to a wide variety of material systems, from simple oxides to mixed metal silicates and phosphates. This route frequently results in metastable phases with interesting physical and chemical properties, from microporous materials to nanoparticles or, as is the case of the present work, magnetic clusterization. It should be pointed out that, while the materials discussed here are analogous to some naturally occurring minerals, the possibility of synthesizing them

* Corresponding author. Tel.: +351 914 419 527.
E-mail addresses: marior@fis.ua.pt, marior@ua.pt (M.S. Reis).

0022-4596/$ - see front matter © 2008 Elsevier Inc. All rights reserved.
doi:10.1016/j.jssc.2008.10.024

in laboratory open doors to tailor their properties chemically/structurally, and potentially perform systematic studies on their magnetic properties.

This report is organized as follows: firstly, the synthesis method and the crystal structure are described, secondly then the magnetic properties will be presented and modeled. Thirdly, the relationship between magnetic properties and the crystal structure will be discussed and, finally, a summary and conclusions of the work will be presented.

2. Experimental procedures

All samples were synthesized in Teflon-lined autoclaves under static hydrothermal conditions at 230 °C during 7 days. Chemicals were purchased from commercial sources; sodium silicate solution (Na_2O 8 wt%, SiO_2 27 wt%, Merck); KOH (Pronalab), KCl (Panreac), $Cu(SO_4)\cdot 5H_2O$ (Pronalab), $(NH_4)_2Fe(SO_4)_2\cdot 6H_2O$ (Merck), $Mn(SO_4)\cdot 4H_2O$ (Merck).

Litidionite synthesis: An alkaline solution was prepared by mixing 6.00 g of a sodium silicate solution, 40.18 g of H_2O, 1.13 g of KOH and 2.70 g of KCl. A second solution was prepared by mixing 20.76 g of H_2O with 1.0 g of $Cu(SO_4)\cdot 5H_2O$. These two solutions were mixed and stirred thoroughly until a homogeneous gel was obtained, with a molar composition of $1 : CuO : 6.75SiO_2 : 1.93Na_2O : 7.03K_2O : 846.40H_2O$.

Fenaksite synthesis: An alkaline solution was prepared by mixing 6.02 g of a sodium silicate solution, 32.26 g of H_2O, 1.86 g of KOH and 2.71 g of KCl. A second solution was prepared by mixing 28.21 g of H_2O with 1.62 g of $(NH_4)_2Fe(SO_4)_2\cdot 6H_2O$. These two solutions were mixed and stirred thoroughly until a homogeneous gel was obtained, with a molar composition of $1 : FeO : 6.54SiO_2 : 1.86Na_2O : 8.42K_2O : 813.41H_2O$.

Manaksite synthesis: An alkaline solution was prepared by mixing 6.00 g of a sodium silicate solution, 15.32 g of H_2O, 0.80 g of KOH and 3.05 g of KCl. A second solution was prepared by mixing 14.80 g of H_2O with 1.04 g of $Mn(SO_4)\cdot 4H_2O$. These two solutions were mixed and stirred thoroughly until a homogeneous gel was obtained, with a molar composition of $1 : MnO : 5.74 SiO_2 : 1.75Na_2O : 5.87K_2O : 355.32H_2O$.

Single crystal X-ray data were collected on a CCD Bruker APEX II using graphite monochromatized Mo-$K\alpha$ radiation ($\lambda = 0.71073$ Å) with the crystal positioned at 35 mm from the CCD. The frames were measured using a counting time of 30, 10 and 80 s for Cu, Fe and Mn samples, respectively. Data reduction and empirical absorption correction were carried out using the SAINT-NT from Bruker AXS. The structure was solved by direct methods and by subsequent difference Fourier syntheses and refined by full matrix least squares on F^2 using the SHELX-97 system programs. The magnetization measurements were performed using a VSM and a quantum design SQUID magnetometers. The susceptibility was measured at 1000 Oe and the magnetization curves at 50 K.

The crystallographic data of the Cu, Fe and Mn samples are summarized in Table 1. *M*–O–*M* bond lengths and angles for the three samples are listed in Table 2. The crystal structures refined in the scope of this work are in agreement with those reported in the JCPDS database: litidionite (JCPDS card 04-010-2767), fenaksite (JCPDS card 04-009-8683) and manaksite (JCPDS card 00-046-1482). Powder diffraction and SEM imaging of the three samples did not show the presence of any impurity phase.

3. Crystal structure

All three compounds characterized in this work are isostructural, differing only in the transition metal (Litidionite—Cu, Fenaksite—Fe, and Manaksite—Mn). These—along with Agrellite, $NaCa_2Si_4O_{10}F$—are the sole members of the Inosilicate class, characterized by tubular or columnar corner sharing SiO_4 tetrahedra. Fenaksite was first described in 1959 by Dorfman [13]. Its crystal structure was determined by Golovach [14] and then refined in 2004 by Rozhdestvenskaya [15]. The structure of litidionite was determined to be isostructural with fenaksite by

Table 2
M–O–*M* bond lengths and angles for Cu, Fe and Mn analogues of the minerals litidionite, fenaksite and manaksite, respectively.

	Cu	Fe	Mn
M–O equatorial (Å)	1.971	2.070	2.122
M–O apical (Å)	2.557	2.282	2.296
Jahn–Teller ratio	1.298	1.102	1.082
M–O–*M* angle (deg)	96.82	99.82	97.88

Table 1
Crystallographic data of Cu, Fe and Mn analogues of the minerals litidionite, fenaksite and manaksite, respectively.

	Cu	Fe	Mn
Empirical formula	$CuKNaSi_4O_{10}$	$FeKNaSi_4O_{10}$	$MnKNaSi_4O_{10}$
Formula weight (g/mol)	397.99	393.30	389.39
Crystal system	Triclinic	Triclinic	Triclinic
Space group	$P\bar{1}$	$P\bar{1}$	$P\bar{1}$
a (Å)	6.9704(4)	6.9742(3)	6.9851(6)
b (Å)	8.0111(5)	8.1326(3)	8.1825(7)
c (Å)	9.7896(9)	9.9301(4)	9.9747(1)
α (deg)	105.56(0)	105.78(0)	105.70(0)
β (deg)	99.53(0)	100.06(0)	99.51(1)
γ (deg)	114.16(0)	114.26(0)	114.58(0)
V (Å^3)	456.32(1)	467.05(6)	473.33(9)
Z	2	2	2
Crystal size (mm)	$0.10\times0.06\times0.04$	$0.20\times0.08\times0.04$	$0.16\times0.01\times0.01$
Crystal type	Blue parallelepiped	Colorless columnar	Pink needle
No. of reflections measured	7813	29 388	5595
Unique reflections	2696	7106	2097
R_{int}	0.0298	0.0310	0.0565
R_1[a], $wR_2[I_0>2\sigma(I_0)]$[b]	0.0492, 0.1449	0.0297, 0.0635	0.0489, 0.0933
R_1, wR_2 (all data)	0.0602, 0.1491	0.0451, 0.0682	0.0912, 0.1053

[a] $R_1 = \sum \|F_0| - |F_c\| / \sum |F_0|$.
[b] $wR_2 = [\sum w(F_0^2 - F_c^2)^2 / \sum w(F_0^2)^2]^{1/2}$.

Pozas in 1975 [16]. It was synthesized first by Guth in 1976 [17], and later by Hefter in 1982 [18]. According to Zamborini [19], the name litidionite was given by E. Scacchin in 1880 to very tiny blue crystals associated with the glass of the same color in lapilli found in the Vesuvius crater. There is relatively little information about Manaksite, its first report dates only from 1992 [20].

In this structure, the repeat unit of Inosilicate characteristic columnar motif, runs along the [100] direction and consists of a set of eight corner sharing SiO_4 tetrahedra, forming two four-member rings and two six-member rings, as shown in Fig. 1(a). Along the chain direction there are eight-member rings as can be seen in Fig. 1(b). This structural element propagates in a direction perpendicular to its six-member ring shown Fig. 1(c).

The metal centers are in square pyramidal coordination, and are arranged in edge-sharing dimers, as depicted in Fig. 2(a). These dimers are magnetically isolated from each other, being separated by, at least, two corner sharing SiO_4—Fig. 2(b). It is also worthy of note that, despite the dimeric arrangement, there is only one crystallographically independent metal position, since the inversion center of the triclinic cell lies in the midpoint of the metal–metal bond.

Each square pyramid is distorted both due to the Jahn–Teller effect (when active) and to its structural environment. Litidionite shows a typical Jahn–Teller distortion, as expected from a Cu^{2+}-$3d^9$ ion. In Fenaksite, although the Fe^{2+}-$3d^6$ is somewhat Jahn–Teller active, no such distortion is observed. Interestingly, in the Mn compound the long bond does not lie perpendicular to the square plane; indicating that the Jahn–Teller contribution to the distortion is less important than the overall structure distortion. In addition, one can consider this SiO_4−MO_5 connectivity as an open framework with small pores where the charge balancing cations, Na^+ and K^+ are located (Fig. 2(c)). The local metal environment for each compound is summarized in Table 2.

4. Magnetic properties

Magnetization measurements as a function of applied magnetic field at 50 K, displayed in Fig. 3 show a linear behavior up to 10 T, this is characteristic of paramagnetic materials or weakly interacting cluster systems.

Susceptibility measurements at high temperature follow the Curie–Weiss law, as expected from magnetically isolated ions. In order to eliminate the temperature-independent diamagnetic contribution, the paramagnetic effective moment p_{eff} and the paramagnetic Curie temperature θ_p were determined from linear fits to the $|d\chi/dT|^{-1/2}$ plot, as shown in Fig. 4. The resulting values are presented in Table 3. The deviation of the experimental p_{eff} from the corresponding theoretical values (using Landé factor $g = 2$ and the orbital angular moment $L = 0$) is a strong indication that there is a significant orbital contribution to the total angular moment in these compounds; however, these are not possible to quantify from magnetization measurements alone. The value of $\theta_p = -17.8(4)$ K (for the manaksite) and $\theta_p = -1.4(1)$ K (for the litidionite) indicate that the intra-dimer interactions are AF. Conversely, intra-dimer interactions for the fenaksite are ferromagnetic, as seen by the positive paramagnetic Curie temperature $\theta_p = +12.0(9)$ K. This observation is confirmed by the magnetization measurements that show, in spite of the higher spin state of the Mn^{2+} ions ($S = \frac{5}{2}$), that the Mn-compound has a lower magnetization at 10 T than the Fe-counterpart ($S = 2$).

In low-dimensional magnetic systems the plot of χT as a function of temperature is also an important quantity to understand their magnetic behavior. In this sense, Fig. 5 presents these curves for all compounds. The positive derivative at lower temperatures observed for the Mn- and Cu-samples is in agreement with the AF arrangement within dimers [2]. For the Fe-counterpart a quite different behavior was found. The χT plot shows a maximum at 9 K followed by a sharp drop. This peak corresponds to a transition to a three-dimensional state, below which the energy of inter-dimer exchange interactions is comparable to the thermal energy. For temperatures higher than 9 K, the negative derivative of χT is another signature of ferromagnetic alignment within the dimers. It is also important to emphasize that we have measured the field-cooled (FC) and zero-field-cooled (ZFC) of these materials and there is no thermal irreversibility nor blocking temperature for the three materials.

Quantitatively speaking, it is possible to use the Heisenberg–Dirac–Van Vleck (HDVV) Hamiltonian to explain the magnetic susceptibility of the dimeric units. This Hamiltonian

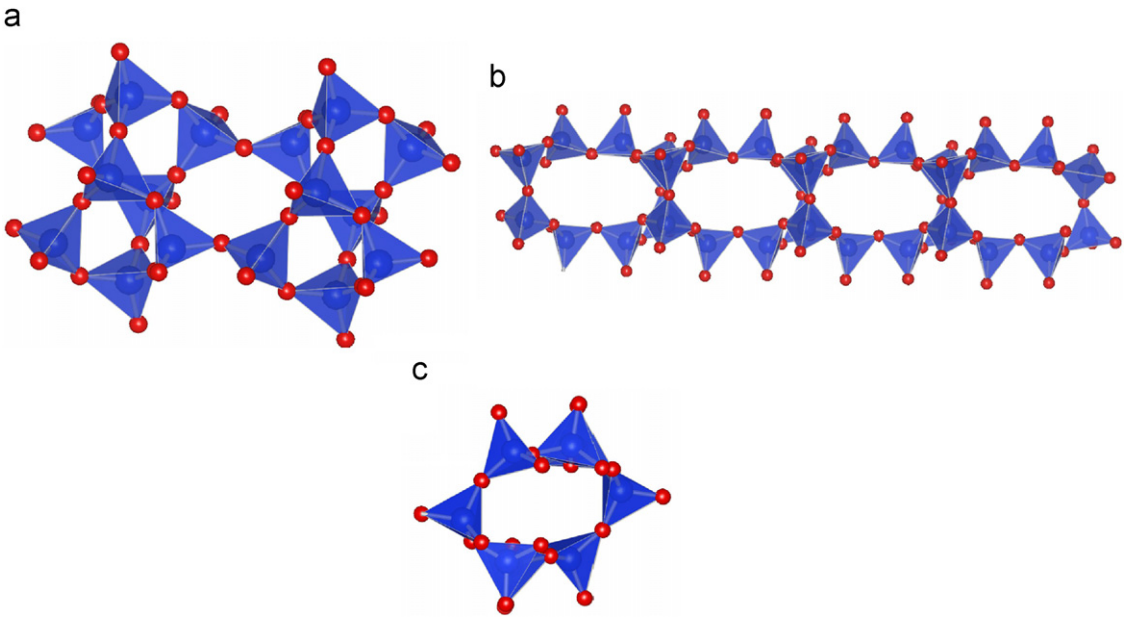

Fig. 1. (Color online) Details of the silicate network of the reported compounds. Two adjacent repeat units are shown in (a). The side view of the columnar SiO_4 network is presented in (b). In (c) a cut normal to the propagation direction is shown, highlighting the six-member ring.

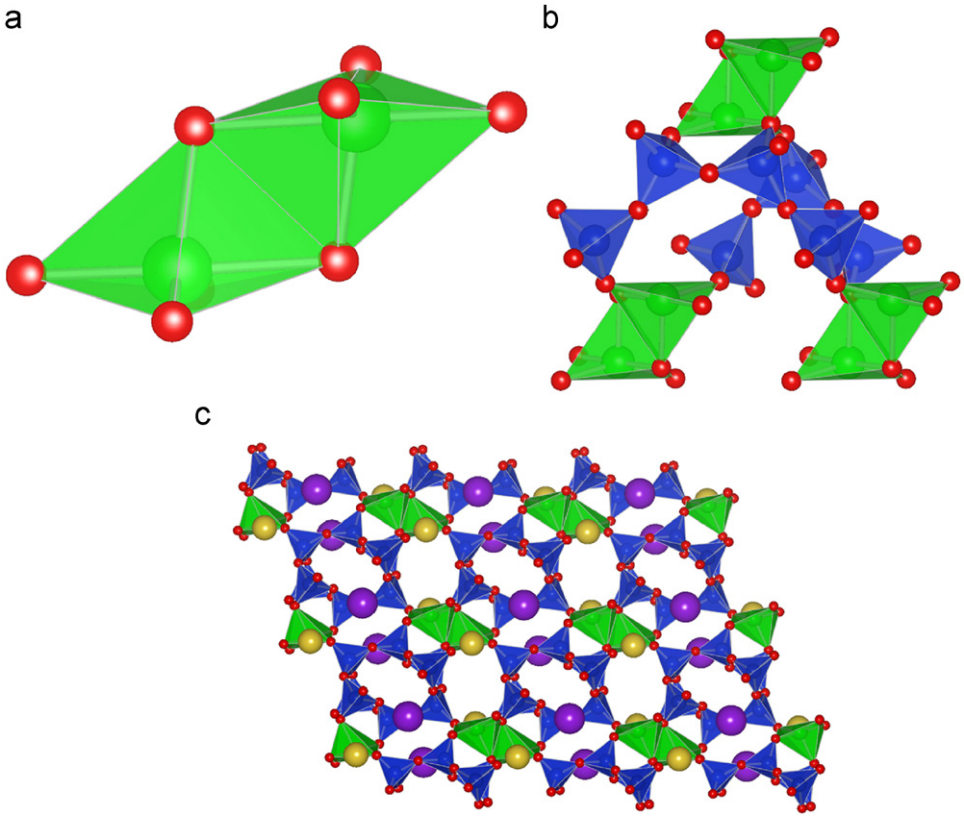

Fig. 2. (Color online) (a) M_2O_8 (M = Mn, Fe and Cu) dimeric unit, note the distortion of the MO_5 unit and the apical–equatorial (*cis*) edge-sharing arrangement; (b) dimer–dimer connectivity; (c) three-dimensional network connectivity.

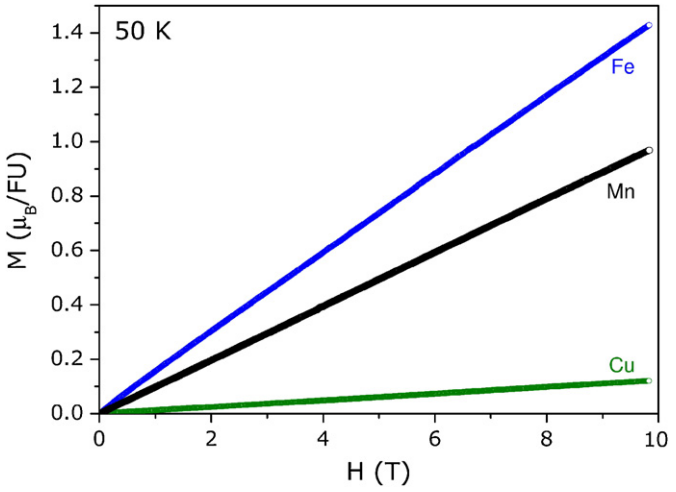

Fig. 3. (Color online) Magnetization as a function of applied magnetic field, up to 10 T and at 50 K, for $KNaMSi_4O_{10}$ (M = Fe : fenaksite, Cu:litidionite and Mn:manaksite). In spite of the higher spin value of the Mn^{2+} ions ($S=\frac{5}{2}$), manaksite has a total magnetic moment lower that the Fe-counterpart ($S=2$). This feature arises due to the antiparallel alignment between the Mn ions within the dimeric unit (see text for details).

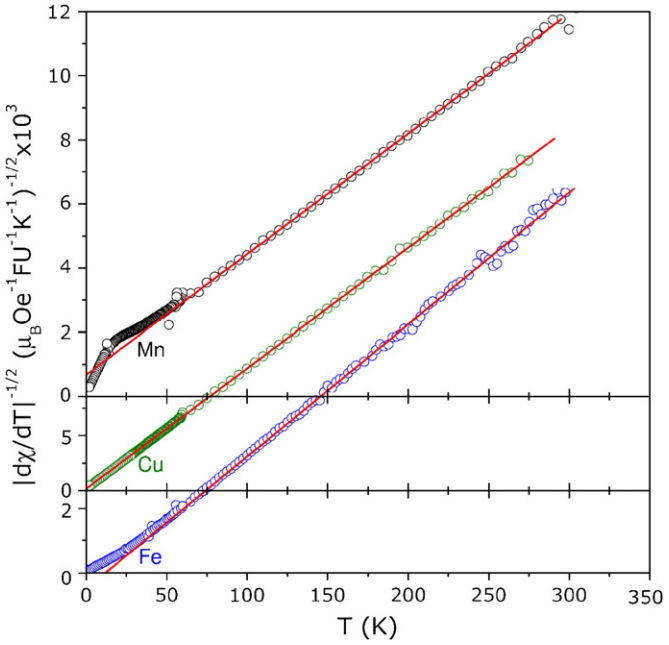

Fig. 4. (Color online) Plot of $|d\chi/dT|^{-1/2}$ to suppress the temperature-independent diamagnetic contribution and to extract the paramagnetic Curie temperature θ_p and paramagnetic effective moment p_{eff} (see Table 3). The deviation from the Curie Law below 50 K is due to the intra-dimer exchange interactions.

corresponds to [2]

$$\mathscr{H} = -J\vec{S}_A \cdot \vec{S}_B \tag{1}$$

where J is the exchange parameter and $\vec{S}_A$ and $\vec{S}_B$ the spins of each metal of the dimeric unit. However, since the Fe mineral has a inter-dimer interaction superimposed to the intra-dimer interaction (as evidenced by the onset of three-dimensional order), a more general expression to the above Hamiltonian, considering a mean-field approximation should be applied. In this case, Eq. (1) can be rewritten as [2]

$$\mathscr{H} = -JS_A \cdot S_B - \mathfrak{z}J'\langle S_z\rangle S_z \tag{2}$$

Table 3
Summary of the parameters obtained fitting Eq. (6) to the magnetic susceptibility data (see Fig. 5).

	Cu ($S=\frac{1}{2}$)	Fe ($S=2$)	Mn ($S=\frac{5}{2}$)
p_{eff} (exp) (μ_B)	1.93(9)	5.1(5)	5.6(4)
p_{eff} (teo) (μ_B) ($g=2$, $L=0$)	1.73	4.90	5.92
θ_p (K)	−1.4(1)	+12.0(9)	−17.8(4)
J (K)	−2.86(3)	+7.6(1)	−3.83(1)
$\jmath J'$ (K)	–	0.222(6)	–
g	1.555(1)	1.468(2)	1.3005(5)
χ_D (μ_B Oe^{-1} FU^{-1}) × 10^{-9} at 1 kOe	−8.5(5)	$\ll 10^{-9}$	$\ll 10^{-9}$
M–O–M bond angle (deg)	96.82	99.82	97.88
Magnetic order within dimers	Antiferromagnetic	Ferromagnetic	Antiferromagnetic

p_{eff} stands for the paramagnetic effective moment, θ_p: paramagnetic Curie temperature, J: intra-dimer exchange interaction, J': inter-dimer exchange interaction, $\jmath$: the number of nearest neighbors around a given dimer, g: Landé factor and, finally, χ_D: temperature-independent diamagnetic susceptibility.

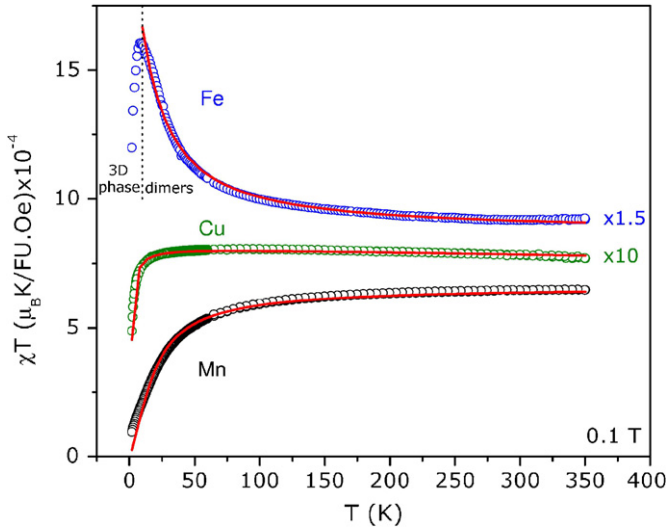

Fig. 5. (Color online) Plot of χT versus T. The antiferromagnetic arrangement within Mn and Cu dimers is evident (due to the positive derivative at lower temperatures). For the Fe-counterpart a three-dimensional transition to an antiferromagnetic inter-dimer interaction is found upon cooling. Above this transition the drop in χT is a signature of ferromagnetic intra-dimer interactions.

where J' is the exchange interaction between nearest neighbor dimers, $\jmath$ the number of nearest neighbors around a given dimer and $\langle S_z \rangle$ is the mean value of the z component of the $S = S_A + S_B$ operator. The magnetic susceptibility is (for the $S_A = S_B$ case) [2]

$$\chi(J,T) = \frac{Ng^2\mu_B^2 F(J,T)}{k_B T - zJ' F(J,T)} \tag{3}$$

where

$$F(J,T) = 2\frac{e^x + 5e^{3x} + 14e^{6x} + 30e^{10x} + 55e^{15x}}{1 + 3e^x + 5e^{3x} + 7e^{6x} + 9e^{10x} + 11e^{15x}} \tag{4}$$

$x = J/k_B T$ and g stands for the Landé factor. This expression is valid for dimers with $S_A = S_B = \frac{5}{2}$. For any $S_A (= S_B)$ value, ranging from $\frac{1}{2}$ up to $\frac{5}{2}$, minor changes must be done in the above equation. For $S_A = S_B = \frac{5}{2} - \frac{1}{2} = 2$ the last term of the numerator and denominator must be suppressed. For $S_A = S_B = 2 - \frac{1}{2} = \frac{3}{2}$ the last terms of the numerator and denominator must be suppressed again. This procedure is valid down to $S_A = S_B = \frac{1}{2}$, where the $F(J,T)$ is simply:

$$F(J,T) = \frac{2}{3 + e^{-x}} \tag{5}$$

In addition to fully describe the magnetic susceptibility of these compounds, a temperature-independent diamagnetic contribution χ_D must be added to Eq. (3). The final equation to appropriately fit the experimental data is therefore:

$$\chi_{total}(J,T) = \chi(J,T) + \chi_D \tag{6}$$

The fits to the data are displayed in Fig. 5 and the obtained fitting parameters are in Table 3. The low values of the Landé factor g are not surprising since the values of the effective moment for each magnetic ion, extracted from the Curie–Weiss law, was somewhat different from the theoretical expected value, indicating therefore an orbital contribution L to the total angular moment. The values of the intra-dimer exchange parameter J are also in agreement with the previous fits to the high temperature susceptibility data, in which we concluded that the Mn- and Cu-compounds have an AF arrangement within those dimers; while a ferromagnetic arrangement is observed in Fe-counterpart. The number of nearest neighbors around a given dimer $\jmath$ times the inter-dimer exchange parameter J' is also a fitting parameter and was used only for the Fe-compound. Due to the weak inter-dimer interactions, $|J| \gg |\jmath J'|$ as expected [2].

5. Structure-magnetism relationship

While the intra-dimer exchange in all the compounds is rather weak, there are other instances where transition metals with similar coordination have much larger magnetic exchange [21]. This intrinsic weakness of the exchange can be understood by observing that (i) these metal ions are in a distorted environment and that typically weakens magnetic interactions and (ii) the connectivity within the dimers is of *cis* type (i.e. the shared edge is between an equatorial oxygen, that lies in the base of the square pyramid, and the apical one). This type of shared edge arrangement is characterized for its weak magnetic interactions, because the magnetically active $d_{(x^2-y^2)}$ orbital in every CuO_5 polyhedron does not overlap as much as in the *trans* arrangement (where the shared edge belongs to the square plane containing the $d_{(x^2-y^2)}$ orbital). A notable example of this effect is present in $Na_2Cu_2Si_4O_{11}$ where alternation between *cis* and *trans* edge-sharing octahedra causes a strongly dimerized chain, despite very similar Cu–Cu distances along the chain [22].

Given such a weak intra-dimer interaction the absence of long range order in both the copper and manganese compounds is not surprising, particularly considering that the intra-dimer AF interaction results in an $S = 0$ cluster connected through an Si_2O_8 unit as highlighted in Fig. 2b. The three-dimensional ordering of

the iron compound can be understood in light of the intra-dimer ferromagnetic exchange (overall cluster spin $S = 4$) in the Fe_2O_8 cluster. As it was demonstrated above, these clusters order at sufficiently low temperature. However, considering the distance between dimers, together with the low exchange value extracted from the fits to the susceptibility data, one can suggest that this ordering mechanism is not due to a superexchange mechanism but more likely has a dipolar origin.

The magnetic arrangement within dimers can also be understood in the context of the structure in the light of the Goodenough–Kanamori rules [8–10]. For edge-sharing polyhedra (M–O–M bond close to 90°) it is predicted that the exchange should be weakly ferromagnetic for undistorted bonding (due to strict orthogonality of the occupied orbitals) and as the distortion increases (and consequently the orbital overlap) the exchange changes sign to become AF. In a recent paper, Reis et al. [23,24] (and references therein) confirmed that the crossover angle Cu–O–Cu above which AF interactions takes over is around 97°, in accordance therefore with the reported structure for Litidionite [16] (Cu–O–Cu is about 96.82°). The weak Cu–Cu interaction ($J = -2.86(3)$ K) is due to the fact that the measured Cu–O–Cu bond angle is quite close to that crossover angle compounded by the abovementioned structural distortion. On the other hand, the ferromagnetic interaction observed in the Fe-compound is more unusual. While FM dimer systems have been described before in distorted Cu [23] and Mn [25] compounds, in iron(II) this observation is rare. In fact first principles calculation of Fe_4O_{20} clusters indicate that such alignment is not expected in any angular range [26]. It would be interesting to obtain high resolution crystallography data in order to understand the structural origin of this FM alignment from theory.

6. Conclusions

In the present work the synthesis and magnetic properties of three isostructural transition metal silicates was described. The distortion present in the structure arises not only from Jahn–Teller effect of the transition metals but also from the inherent complexity of the structure and allows for the observation of interesting magnetic behavior. Both Cu and Mn compounds have intra-dimer AF interaction, while Fe is somewhat surprisingly ferromagnetic. While this is an unusual observation, it is interesting to observe that the overall $S = 4$ low temperature cluster of this compound allows for three-dimensional ordering at low temperature. The magnetism was successfully modeled using an HDVV formalism with an added mean field term to account for the three-dimensional transition in fenaksite and interpreted in the light of the crystal structure, with respect to the ferro and antiferro arrangements as a function of the crystalline distortion.

Acknowledgment

Research sponsored by the Laboratory Directed Research and Development Program and the Division of Materials Sciences and Engineering, of Oak Ridge National Laboratory (ORNL), managed by UT-Battelle, LLC for the U.S. Department of Energy under Contract no. DE-AC05-00OR22725. The authors also thank FCT for the VSM equipment (REEQ/1126/2001). One of the authors (M.S.R.) acknowledges the financial support from the PCI Program during his stay at CBPF.

References

[1] J. Miller, M. Drillon, Molecules to Materials, Wiley-VCH, New York, 2001.
[2] O. Kahn, Molecular Magnetism, Wiley-VCH, New York, 1993.
[3] A. Rocha, V. Garcia-Suarez, S. Bailey, C. Lambert, J. Ferrer, S. Sanvito, Nat. Mater. 4 (2005) 335.
[4] A. Souza, M. Reis, D. Soares-Pinto, I. Oliveira, R. Sarthour, Phys. Rev. B 77 (2008) 104402.
[5] M. Verdaguer, Polyhedron 20 (2001) 1115.
[6] M. Hase, I. Terasaki, K. Uchinokura, Phys. Rev. Lett. 70 (1993) 3651.
[7] J.F. DiTusa, S.W. Cheong, J.H. Park, G. Aeppli, G. Broholm, C.T. Chen, Phys. Rev. Lett. 73 (1994) 1857.
[8] J. Goodenough, J. Phys. Chem. Solids 6 (1958) 287.
[9] J.B. Goodenough, Phys. Rev. 100 (1955) 564.
[10] J. Kanamori, J. Phys. Chem. Solids 10 (1959) 87.
[11] P. Hay, J. Thibeault, R. Hoffmann, J. Am. Chem. Soc. 97 (1975) 4884.
[12] J. Glerup, A. Patricia, J. Derek, M. Kirsten, Inorg. Chem. 34 (1995) 6255.
[13] M. Dorfman, D. Rogachev, Z. Goroshchenko, A. Mornnrsovt, Mineralog. Muzeya Akod. Nauk SSSR 9 (1959) 152.
[14] V. Golovach, Y. Drozdov, E. Kuzmin, Dokl. Akad. Nauk SSSR 194 (1970) 818.
[15] I. Rozhdestvenskaya, I. Bannova, L. Nikishova, Dokl. Earth Sci. 398 (2004) 1029.
[16] J. Pozas, G. Rossi, V. Tazzoli, Am. Mineralog. 60 (1975) 471.
[17] Guth, C.R. Acad. Sci. Ser. D 285 (1977) 1221.
[18] J. Hefter, M. Kenney, Inorg. Chem. 21 (1982) 2810.
[19] F. Zamborini, Mineralogia Vesuuiana, S.I.E.M., Napoles, 1935, p. 435.
[20] A. Khomyakov, T. Kurova, G. Nechelyustov, Zap. Vses. Mineral. Obshch. 121 (1992) 112.
[21] A. Belik, H. Koo, M. Whangbo, N. Tsujii, P. Naumov, E. Takayama-Muromachi, Inorg. Chem. 46 (2007) 8684.
[22] A.M. dos Santos, V. Amaral, P. Brandao, F. Paz, J. Rocha, L. Ferreira, M. Godinho, O. Volkova, A. Vasiliev, Phys. Rev. B 72 (2005) 092403.
[23] M. Reis, A.M. dos Santos, V. Amaral, P. Brandăčo, J. Rocha, Phys. Rev. B 73 (2006) 214415.
[24] A.M. dos Santos, P. Brandao, A. Fitch, M.S. Reis, V.S. Amaral, J. Rocha, J. Solid State Chem. 180 (2007) 16.
[25] Cao, Inorg. Chem. 46 (2007) 428.
[26] T. Cauchy, E. Ruiz, S. Alvarez, J. Am. Chem. Soc. 128 (2006) 15722.